The variable N terminal region of DDX5 contains structural elements and auto-inhibits its interaction with NS5B of hepatitis C virus

Sujit Dutta[1,2,*], Garvita Gupta[3,*], Yook-Wah Choi[1,4], Masayo Kotaka[5], Burtram C. Fielding[4], Jianxing Song[3,6], Yee-Joo Tan[1,7, §]

[1]Institute of Molecular and Cell Biology, A*STAR (Agency for Science, Technology and Research), Singapore, [2]School of Life Sciences and Chemical Technology, Ngee Ann Polytechnic, Singapore, [3]Department of Biological Sciences, Faculty of Science, National University of Singapore, [4]Molecular Virology Laboratory, Department of Medical BioSciences, University of the Western Cape, South Africa, [5]Department of Physiology, Li Ka Shing Faculty of Medicine, University of Hong Kong, Hong Kong, [6]Department of Biochemistry and [7]Department of Microbiology, Yong Loo Lin School of Medicine; National University of Singapore,Yong Loo Lin School of Medicine, National University Health System (NUHS), National University of Singapore.

* These authors contributed equally to this work

§Correspondence to:
Address: MD4, 5 Science Drive 2, Singapore 117597
E-mail: Yee_Joo_TAN@NUHS.edu.sg
Tel: (65) 65163692
Fax: (65) 67775720

Short title: Structure of part of the variable N terminal region and domain 1 of DDX5

Accession Number:
The structure of the N-terminal domain of DDX5 has been deposited in the Protein Databank under ID code 4a4d.

Abbreviations:
HCV, hepatitis C virus; aa, amino acids; NTR, N terminal region; DTT, dithiothreitol; GST, glutathione S-transferease; HSQC, Heteronuclear Single Quantum Coherence; T2, transverse relaxation time.

Abstract (199 words)

RNA helicases of the DEAD-box family of proteins are involved in many aspects of RNA metabolism from transcription to RNA decay but most of them have also been shown to be multi-functional. A member DDX5 has been shown to interact with the RNA-dependent RNA polymerase (NS5B) of hepatitis C virus. Here, we report the presence of two independent NS5B binding sites in DDX5, one located at the N terminus and another at the C terminus. The N-terminal fragment of DDX5, DDX5-N, was crystallized and the structure of domain 1 of DDX5 shows typical features found in the structures of other DEAD-box helicases. DDX5-N contains the highly variable N terminal region (NTR) of unknown function and the crystal structure reveals structural elements in part of the NTR, namely residues 52-78. This region forms an extensive loop and an α-helix. From co-immunoprecipitation experiments, the NTR of DDX5-N was observed to auto-inhibit its interaction with NS5B. Interestingly, the α-helix in NTR is essential for this auto-inhibition and seems to mediate the interaction between the highly flexible 1-60 residues in NTR and NS5B binding site in DDX5-N. Furthermore, NMR investigations reveal that there is a direct interaction between DDX5 and NS5B *in vitro*.

Introduction

Hepatitis C is an infectious disease affecting an estimated 150-200 million people worldwide. Infection is caused by the hepatitis C virus (HCV), which can often lead to cirrhosis, steatosis, and hepatocellular carcinoma. HCV is an enveloped, single stranded positive-sense RNA virus in the family *Flaviviridae* [1]. The viral genome is encoded by three structural proteins (core, E1 and E2) and seven non-structural proteins (p7, NS2, NS3, NS4A, NS4B, NS5A and NS5B). NS3, a serine protease and RNA helicase, along with NS5B, an RNA-dependent RNA polymerase, are key enzymes required for HCV replication and therefore common targets for antiviral agents. Viral replication requires interaction between RNA, viral and host proteins [1]. NS5B has been shown to interact with a growing number of host proteins including eukaryotic initiation factor 4AII [2], cellular vesicle membrane transport protein VAP-33 [3], nucleolar phosphoprotein nucleolin I [4] and the DEAD (Asp-Glu-Ala-Asp) box RNA helicase DDX5 [5].

DDX5, also referred to as p68, is a nuclear prototypic member of the DEAD-box family of proteins. The DEAD-box family belongs to helicase superfamily 2 (SF2), which also includes DEAH, DExH and DExD families (see recent reviews by [6-8]). DEAD-box helicases share nine conserved motifs that are clustered in a central region and possess highly variable amino and carboxyl termini. The central region of DEAD-box helicases region can be organized into two domains; domain 1 consists of motifs Q, I (Walker A), II (Walker B, DEAD box), Ia, Ib and III while domain 2 consists of motifs IV, V, and VI. Motif Q, which is unique to DEAD-box helicases, forms the nucleotide binding site together with motifs I and II. Motif III has been implicated in linking ATP binding and hydrolysis with the helical activity. The remaining motifs are involved in RNA binding. The functions of the variable N and C terminal regions are not fully characterized but they are thought to interact with RNA substrates or co-factors so as to confer specificity or fine modulation of function.

DDX5 was first identified by its immunological cross-reactivity to a monoclonal antibody to the large T antigen of simian virus 40 [9]. Co-purification of DDX5 with splicesomes initially suggested a role in RNA splicing and this was subsequently confirmed when DDX5 was shown to be an essential splicing protein acting at the U1 snRNA-5' splice site [10]. DDX5 has also been shown to be involved in RNA export, ribosome assembly, translation and RNA degradation [6, 11-12]. However, there is a growing body of evidence suggesting DDX5 has an additional role as a transcriptional co-activator for different genes [13].

DDX5 has been shown to interact with HCV NS5B and the knockdown of DDX5 by RNA interference caused a reduction in the transcription of negative-strand HCV RNA [5]. Furthermore, the over-expression of NS5B has been shown to result in the redistribution of DDX5 from the nucleus to the cytoplasm [5] and interestingly, DDX5 was also found to have undergone similar translocation in HCV infected cells [14]. In addition, single nucleotide polymorphisms in DDX5 gene have been shown to be significantly associated with increased risk of advanced fibrosis in HCV patients [15]. While the precise role of DDX5 in HCV infection has yet to be defined, these studies suggest that it may play an important role in HCV replication.

In order to gain an understanding into the mechanism of interaction between DDX5 and NS5B, we expressed DDX5(1-305 amino acids (aa)) and obtained the crystal structure of part of the variable N terminal region (NTR) and domain 1 (residues 52 to

304) at 2.7 Å resolution. The residues in DDX5 involved in the interaction with NS5B were also evaluated by using site-directed mutagenesis and co-immunoprecipitation experiments. Furthermore, NMR investigations were performed to determine if there is a direct interaction between DDX5 and NS5B.

Materials and Methods
Mammalian expression constructs

The open reading frame encoding human DDX5 was amplified from a spleen cDNA expression library [5]. DDX5 was cloned into pXJ40myc, a myc-tagged plasmid derived from pXJ40 [16]. DDX5 deletion and substitution mutants were generated by polymerase chain reaction. NS5B was amplified from the cDNA of HCV-S1 of genotype 1b [17], and cloned into pXJ40flag, a flag-tagged plasmid derived from pXJ40 [16].

Transfection, co-immunoprecipitation and Western Blot analysis

Huh-7 cells (human hepatoma, JCRB Cell Bank) were cultured in Dulbecco's Minimal Eagle's medium supplemented with 10 % fetal bovine serum (HyClone Laboratories) and antibiotics, penicillin at 10 Units/ml and streptomycin at 100 μg/ml (Sigma), and maintained at 37°C in 5% carbon dioxide.

Plasmids were transiently transfected into Huh-7 cells plated in 6-cm^2 tissue culture dishes using Lipofectamine (Invitrogen), according to the manufacturer's instruction. The cells were harvested ~24 h post-transfection and lysed in 150 μl of RIPA buffer (50 mM Tris-HCl, pH 7.4, 150 mM NaCl, 0.5% (v/v) NP-40, 0.5% (w/v) deoxycholic acid, 0.005% (w/v) SDS and 1 mM PMSF) and subjected to three cycles of freezing and thawing. The cell lysates were spun down at 16 000 g for 20 min at 4°C to remove cell debris.

For co-immunoprecipitation, cell lysates were first incubated with 2 μg of anti-myc polyclonal antibody (Santa Cruz) for 1 h at room temperature before mixing with 20 μl pre-washed Protein A-agarose beads (Roche). The mixtures were left to incubate overnight with agitation at 4°C. The protein-bound beads were then washed 4 times with 1 ml RIPA buffer. 5X SDS loading buffer (0.3 M Tris-HCl, pH 6.8, 5% (w/v) SDS, 50% (v/v) glycerol, 0.1 M dithiothreitol (DTT) and 0.1% (w/v) bromophenol blue) was added to the washed beads. The bound proteins were eluted from the beads by boiling the samples at 100°C for 5 min. Similarly, 5X SDS loading buffer was added to aliquots of cell lysates before immunoprecipitation and the samples were boiled at 100°C for 5 min.

All protein samples were resolved on SDS- polyacrylamide gels, transferred onto Hybond-C nitrocellulose membranes (GE Healthcare) and blocked with 5% non-fat milk in PBS with 0.05% (v/v) Tween-20. The membranes were then incubated with primary antibodies (either anti-myc polyclonal antibody (Santa Cruz) or anti-flag monoclonal antibody (Sigma) or anti-flag polyclonal antibody (Sigma)) followed by secondary antibodies conjugated with horseradish peroxidase. The proteins were then visualized with the aid of SuperSignal® West Pico Substrate Kit (Pierce). The chemiluminescent protein signals were captured on Amersham Hyperfilm™ (GE Healthcare).

Expression and purification of bacterially expressed DDX5(1-305aa)

The N-terminal domain of DDX5 (residues 1-305) was expressed as a glutathione S-transferease (GST) (pGEX6p1, GE Heathcare) fusion protein. GST-DDX5(1-305aa) was expressed in *Escherichia coli* BL21-CodonPlus-RIL (Stratagene). Cultures were grown at 37°C in Terrific-Broth medium and on reaching an OD600 of 0.8, cells were cooled to 16°C and induced with isopropyl β-D-1-thiogalactopyranoside to a final concentration of 0.2 mM. After an incubation period of 24 h, cells were harvested. Bacterial pellets were re-suspended in lysis buffer (50 mM Tris-HCl, pH 7.4, 300 mM

NaCl and 2 mM DTT) supplemented with Complete Protease Inhibitor (Roche). For purification, cells were subjected to sonication. The lysate was cleared by centrifugation and loaded onto a 5 ml glutathione sepharose column (GE Healthcare) pre-equilibrated with lysis buffer. The column was washed to remove unbound material. Removal of the GST tag from the N-terminal of DDX5(1-305aa) was achieved by proteolytic cleavage using recombinant 3C protease (GE Healthcare). Cleaved protein was further purified by size-exclusion chromatography using Superdex S200 column (GE Healthcare) pre-equilibrated in lysis buffer. Purified DDX5(1-305aa) was concentrated to 12 mg/ml using Amicon Ultra (10 kDa cutoff, Millipore).

Crystallization and data collection

Crystals of recombinant DDX5(1-315aa) (12 mg/ml) were obtained at 15°C using the sitting-drop vapour diffusion method from 1 : 1 µl of protein and precipitant containing 2% (v/v) Tacsimate (pH 4.0), 0.1 M Bis-Tris (pH 6.5) and 20% (w/v) polyethylene glycol (PEG) 3350. Crystals were transferred to a reservoir solution containing the precipitant with the addition of 30 % glycerol, before flash freezing in liquid nitrogen.

X-ray diffraction data from a single crystal of DDX5(1-305aa) was collected at the National Synchrotron Radiation Research Center (NSRRC, Taiwan) on beamline 13B1. Raw data were integrated and scaled using the HKL2000 program suite [18].

Structure determination and refinement

The structure of DDX5(1-305aa) was determined by the molecular replacement method, using the structure of domain 1 of DDX3X ([19] Protein Data Bank (PDB) code 2I4I) as the search model, with the program Molrep from CCP4 suite [20]. The model was refined with CNS [21], and multiple rounds of manual fitting with the program O [22] using $2F_o$-F_c and F_o-F_c electron density maps. The refined model consists of 57 water molecules, with a final R and R_{free} of 27% and 29% respectively. There is 1 molecule in the asymmetric unit with 253 residues. The stereochemistry of DDX5(1-305aa) was checked with PROCHECK [23]. The refinement statistics are summarized in Table 1.

***In vitro* translation and GST pull-down assay**

pXJ40myc-DDX5(61-614aa) and pXJ40flag-NS5B plasmids were used as templates to produce the ^{35}S-labeled proteins using the TNT reticulocyte lysate system (Promega), according to the manufacturer's protocol.

30 µg of GST and GST fusion proteins bound on glutathione sepharose beads were washed three times with GST pull-down buffer (PBS with 0.5% (v/v) Triton X-100, 0.5% (v/v) NP40, 1 mM EDTA, 1 mM EGTA and 0.4 mM PMSF). 20 µl of ^{35}S-labeled proteins, diluted with 80 µl GST pull-down buffer were added to the beads and the mixtures were incubated at room temperature for 1 h. The beads were then washed 4 times with GST pull-down buffer. 5X SDS loading buffer was added to the beads and the bound proteins were eluted from the beads by boiling at 100°C for 5 min. The samples were resolved on a 10% SDS-polyacrylamide gel. The resolved gel was soaked in a solution of 45% methanol and 10% acetic acid for 30 min and then placed in Amplify™ solution (GE Healthcare) for 30 min. The gel was placed on a piece of filter paper,

covered with cling wrap and dried for 1 h at 80°C in a gel drier. The radiolabelled signals were captured on Amersham Hyperfilm™ (GE Healthcare).

Expression and purification of recombinant proteins for CD and NMR studies

The gene encoding the 570-residue NS5B was PCRed out from the pXJ40flag-NS5B plasmid, which contains NS5B of HCV genotype 1b [5], and then cloned into pET32a. The gene encoding DDX5(61-305aa) was excised by restriction enzyme digestion from the mammalian expression vector described above and cloned into pGEX6p1 vector (GE Heathcare). These two bacterial expression vectors were transformed into *Escherichia coli* BL21 (DE3) Star (invitrogen) cells. For expression of recombinant proteins, cells were grown in Luria-Bertani medium in the presence of ampicillin (100 mg/ml) at 37 °C to reach the absorbance of 0.6 at 600 nm and subsequently induced with respective optimized isopropyl β-D-1-thiogalactopyranoside concentrations. Harvested cells were resuspended and lysed by sonication in lysis buffer (50 mM Tris, pH 7.5, 500 mM NaCl, 10% glycerol, 20 mM imidazole, 10 mM 2-mercaptoethanol) containing protease inhibitor cocktail (Roche). His-tagged NS5B and GST-tagged DDX5(61-305aa) proteins were purified by Ni^{2+}-affinity chromatography (Qiagen) and glutathione sepharose chromatography (GE Healthcare) respectively under native conditions. The recombinant proteins were released from the fused tags by in-gel cleavage with either thrombin (for NS5B) or 3C protease (for DDX5(61-305aa)) and further purified by size-exclusion chromatography using Superdex S200 column (GE Healthcare). The production of the isotope-labeled DDX5(61-305aa) protein for NMR studies followed a similar procedure except that the bacteria were grown in M9 medium with the addition of $(^{15}NH_4)_2SO_4$ for ^{15}N labeling as previously described [24-25]. The concentration of protein samples was determined by the spectroscopic method in the presence of denaturant [24-26].

CD and NMR experiments

All CD experiments were carried out in a Jasco J-810 spectropolarimeter (Jasco Corporation, Tokyo, Japan) as previously described [25] at 25 ºC. The protein concentration is 20 μM in 2 mM phosphate buffer (pH 6.5) for all far-UV CD experiments.

NMR samples were prepared in 10 mM phosphate buffer in the presence of 10 mM DTT (pH 6.5). All NMR data were collected at 25 °C on an 800-MHz Bruker Avance spectrometer equipped with a shielded cryoprobe as previously described [24-25]. For Heteronuclear Single Quantum Coherence (HSQC) characterization of the ^{15}N-labeled DDX5(61-305aa), samples were prepared at a protein concentration of 100 μM. For NMR characterization of the binding interaction of DDX5(61-305aa) to NS5B, one-dimensional ^1H NMR spectra of the DDX5(61-305aa) protein were acquired at a protein concentration of 20 μM in the absence or presence of the unlabeled NS5B at molar ratios of 1:1; 1:2 and 1:3 (DDX5:NS5B). NMR data were processed with NMRpipe [27] and analyzed with NMRview [28].

Results

DDX5 contains two independent NS5B binding sites

To determine which domain(s) in DDX5 are involved in the interaction with NS5B, coimmunoprecipitation experiments were performed using deletion mutants of DDX5. Flag-tagged NS5B was expressed in Huh-7, a liver cell line that supports HCV replication, together with myc-tagged DDX5 proteins (Figure 1). The results showed that two non-overlapping fragments of DDX5, DDX5(61-305aa) and DDX5(306-614aa), bound to NS5B, indicating that there are two independent NS5B binding sites in DDX5. In contrast, DDX5(1-305aa) showed no significant binding to NS5B indicating that the deletion of the N-terminal 60 residues of DDX5(1-305aa) enhanced its binding to NS5B (Figure 1). DDX5(1-305aa) and DDX5(306-614aa) shall be referred to DDX5-N and DDX5-C in this study.

Structural analyses of numerous DEAD-box RNA helicases revealed that they contain a central region comprising of two conserved domains, termed domains 1 and 2, flanked by highly variable N- and C- terminal sequences [19, 29-33]. Bio-informational analysis revealed that DDX5-N and DDX5-C contain domains 1 and 2 respectively (data not shown).

Domain 1 of DDX5 is similar to that of other DEAD-box RNA helicases

To gain further insights into the interaction between DDX5 and NS5B, DDX5-N and DDX5-C were expressed as N-terminal GST fusion. GST was removed with the 3C protease but five amino acids (GPLGS) remained fused to the N-terminal of these proteins. Purification of DDX5-C failed as the protein underwent degradation when expressed in *Escherichia coli* (data not shown). Purification of DDX5-N was successful and crystallization trials were performed. GST-pull down assay was also performed and the results showed that DDX5-N interacts with NS5B (supplementary Figure 1). DDX5-N was found to crystallize in space group *I222* and the structure was solved by molecular replacement using the structure of domain 1 of DDX3X (PDB code: 2I4I) and refined to the crystallographic R-factor of 0.27 (R_{free} 0.29). One molecule was identified in the asymmetric unit. Due to lack of density, residues 1-51 were not observed. The refinement statistics are shown in Table 1.

DDX5-N contains eight centrally located β-sheets packed against nine α-helices (Figure 2). A structure-homology search on the Dali server (www.ebi.ac.uk/dali) reveals a high degree of similarity of domain 1 of DDX5 (residues 79-303) with the equivalent domain in human DDX3X [19], drosophila VASA [32] and eukaryotic initiation factor 4A-I (eIF4a) [30] with a root mean square difference (rmsd) of 1.4 Å, 1.7 Å and 1.9 Å respectively. Structural-based sequence alignment revealed that residues 52-78 of DDX5-N form part of the NTR whereas residues 79-303 correspond to conserved domain 1 (Figure 3). Residues 52-78 of NTR contain a loop and an α-helix whereas the conserved domain 1 displays a RecA-like structure (Figure 3).

It is clear that domain 1 of DDX5 contains many typical features found in the structures of other DEAD box helicases. For example, the conserved motifs, Q, I (Walker A), II (Walker B, DEAD box), Ia, Ib, and III, in domain 1 of DDX5 superimpose with the corresponding regions in DDX3X (Figure 4). The only difference is in the P-loop (found in motif I) because DDX3X is in complex with AMP while DDX5-N is in the apo form. In addition, DDX3X has an insertion between the P-loop and the RNA-

binding motif Ia that forms a helix. It has been suggested this insertion helix is involved in RNA-binding and positioning [19]. This helix is not present in DDX5 (Figure 4).

Recently, the structure of domain 1 of DDX5 in complex with ADP was determined to a resolution of 2.6 Å ([33], PDB code; 3fe2). Structural analyses reveal residues in the Q motif make contact with the adenine moiety of the nucleotide, whereas phosphate moiety makes contact with the P-loop in motif I [33]. Superimposition of the apo and bound form reveals a rmsd of 1.2 Å. Overall, small changes are observed upon ADP binding with the exception of the P-loop. Upon ADP binding, the P-loop shifts by 3.4 Å from the apo form (Figure 5). It is not possible to compare the features in NTR of the two forms because the NTR is absent from the protein used to solve the structure of ADP-bound DDX5 [33].

The ATP binding site of DDX5-N is not essential for the interaction with NS5B

The crystal structure of DDX5-N showed that there is no nucleotide in the ADP/ATP binding site. In order to determine if the ATP binding site of DDX5-N is important for the interaction between DDX5-N and NS5B in Huh-7 cells, co-immunoprecipitation experiments were performed to determine the interaction of two DDX5 substitution mutants (K144N and D248N) with NS5B. Previous study has shown that the K144N substitution abolished ATP-binding while substitution within the DEAD-box did not have any effect on ATP-binding [34]. The DDX5-N(K144N) substitution mutant bound NS5B to a similar extent as DDX5-N suggesting that ATP binding is not essential for the interaction (Figure 6). The DDX5-N(D248N) substitution mutant also showed similar binding to NS5B, suggesting that the DEAD-box is not essential for the interaction.

The flexible region in the NTR of DDX5-N auto-inhibits its interaction with NS5B

The co-immunoprecipitation experiments showed that DDX5-NΔ60 (i.e. DDX5(61-305aa)) binds NS5B stronger than DDX5-N (Figure 1), suggesting that the NTR of DDX5-N can auto-inhibit its interaction with NS5B. However, due to disorder, only part of the NTR region (52-78) was observed in our crystal structure. This region forms an extensive loop and supplements the core with an additional α-helix (Figure 2). Unfortunately, the crystal structure does not reveal any contact between the NTR and the rest of DDX5-N. This does not rule out that the NTR can fold back on the rest of DDX5-N, but rather is a reflection of the highly flexible nature of the NTR and the possibly highly dynamic nature of the interaction. Hence, to further investigate the structural elements in NTR that are involved in the auto-inhibition, coimmunoprecipitation experiments were performed using DDX5-N and 3 mutants of DDX5-N. The first mutant is DDX5-NΔ60 in which the N terminal part of the NTR has been deleted, but the helix in the NTR remains intact. The second mutant is DDX5-NΔ78 where the entire NTR has been deleted. The third mutant is DDX5-NΔ70-78 where the helix in the NTR has been deleted but the flexible first 50 residues and the extended loop remains intact (Figure 7A).

Consistent with the results shown in Figure 1, DDX5-NΔ60aa and DDX5-NΔ78aa showed significantly higher binding to NS5B than DDX5-N (Figure 7B), indicating that the auto-inhibition is abolished when part or the complete NTR is deleted. The internal deletion mutant DDX5-NΔ70-78aa also binds strongly to NS5B (Figure 7B),

indicating that residues 1-69 cannot cause auto-inhibition in the absence of the helix formed by residues 70-78. This suggests that this helix may bring the flexible 1-69 residues of NTR close to the NS5B binding site in DDX5-N, presumably within residues 79-305. Consistently, *in vitro* translated DDX5(61-614aa) was pulled down by DDX5(1-80aa) fused to GST but not by GST alone (Figure 8).

DDX5-NΔ60 interacts directly with NS5B

In order to rule out that the possibility that the auto-inhibition by the NTR of DDX5-N is mediated through the interaction with a third protein, CD and NMR experiments were next performed to characterize the solution conformation of DDX5-NΔ60 and its *in vitro* interaction with NS5B. Firstly, NS5B protein was first expressed and assessed for its solution conformation. As seen in Figure 9A, NS5B has a far-UV CD spectrum typical of a helix-dominant protein, with two large negative signals at ~208 nm and 222 nm respectively, consistent with its three dimensional structure. The very large positive signal at ~192 nm indicates that it also has a tight tertiary packing. A one-dimensional ^{1}H NMR spectrum for NS5B (Figure 9B) was also collected but the resonance peaks are very broad mostly due to the short transverse relaxation time (T2) resulting from its very large size.

Secondly, DDX5-NΔ60 was purified and subjected to far-UV CD spectroscopy (Figure 9A). The results show that DDX5-NΔ60 has a helix-dominant structure with tight tertiary packing, in agreement with its three dimensional structure determined in the present study. Consistent with the CD results, the one-dimensional ^{1}H NMR spectrum of DDX5-NΔ60 shows a large dispersion of the amide protons signals as well as many very up-field signals (Figure 9D), indicating that DDX5-NΔ60 is well folded. However, also likely due to its relatively large size, its proton resonance signals are broad. This is further confirmed by its two-dimensional ^{1}H-^{15}N HSQC spectrum acquired on a ^{15}N-labeled DDX5-NΔ60 sample (Figure 9C), in which although both ^{1}H and ^{15}N spectral dispersion are large, many peaks from amide protons are too broad to be detectable.

As a consequence, the direct binding of DDX5-NΔ60 to NS5B was assessed by monitoring the one-dimensional ^{1}H NMR spectra of DDX5-NΔ60 in the absence or presence of NS5B at molar ratios of 1:1, 1:2 and 1:3 (Figure 9E). Interestingly, addition of NS5B into DDX5-NΔ60 at a molar ratio of 1:1 (DDX5:NS5B) caused a significant decrease of resonance intensities and resulted in resonance broadenings (Figure 9E). Furthermore, no large change was further detected for the NMR spectra when more NS5B was added (at molar ratios of 1:2 and 1:3). This clearly indicates that DDX5-NΔ60 binds to NS5B to form a tight complex because the complex formation was almost completed at a molar ratio of 1:1 (DDX5:NS5B). However, the very large molecular weight of the tight complex will lead to a dramatic shortening of T2, and consequently the NMR signals become very broad, thus leading to the significant reduction of the signal intensity. If no interaction existed between DDX5-NΔ60 and NS5B, the NMR spectrum of the mixture would be a simple addition of two separate spectra which should have resonance intensities larger than each spectrum (Figure 9F). However, this is not the case, demonstrating that DDX5-NΔ60 does interact directly with NS5B.

Further biophysical characterization of the interaction between DDX5-NΔ60 and NS5B was hindered by the fact that the DDX5-NΔ60-NS5B complex appears to be prone to aggregation. Although during the NMR titrations, no visible aggregation was observed,

the mixture sample would precipitate overnight. Indeed, in order to obtain thermodynamic binding parameters, isothermal titration calorimetry was performed with various protein concentrations but all the experiments failed because of sample precipitation. It is likely that the precipitation of the complex was accelerated by rapid spinning of the needle during the isothermal titration calorimetry measurements.

Discussion

Over the past decade, a growing number of DEAD-box RNA helicase structures have been determined [19, 29-33]. They contain a central region comprising of two conserved domains, termed domains 1 and 2, flanked by highly variable N- and C-terminal sequences. Comparison of known structures of domain 1 and 2 reveal they have a fold belonging to the RecA super family, where five β-strands are surrounded by five α-helices [35]. We have previously shown that DDX5 interacts with NS5B and that the C terminal of NS5B is essential for this interaction [5]. Coimmunoprecipitation experiments showed there are two independent NS5B binding sites in DDX5, one in DDX5-N (corresponding to residues 1 to 305 of DDX5) and the other in DDX5-C (corresponding to residues 306 to 614 of DDX5) (Figure 1). Interestingly, DDX5-N and DDX5-C contain domain 1 and 2 respectively.

The crystal structure of the apo form of DDX5-N (residues 52-304) was solved and it reveals that domain 1 of DDX5 contains many typical features found in the structures of other DEAD box helicases (Figures 2 and 3). Generally, the P-loop in DEAD-box helicases adapts either an open or closed conformation. The open conformation, typically found in NTPases whether nucleotide bound or not, is observed in the nucleotide bound form of the DEAD-box helicase eIF4A [30] and 56-kDa U2AF-associated protein UAP56 [31] whereas the closed conformation is observed in the unbound structures of eIF4A [30], UAP56 [31], and BSTDead [29]. In DDX5-N, the P-loop clearly adopts an open conformation in the presence of bound nucleotide whereas the apo form is in a closed conformation (Figures 4 and 5). However, neither the ATP binding site nor DEAD motif in DDX5-N is required for its interaction with NS5B (Figure 6).

The NTRs of DEAD-box helicases are highly variable and there is limited structural information [6-7]. For DDX5-N, no density was observed for residues 1-51 within the NTR. Analysis, using the protein disorder server RONN [36], predicted this region to be disordered as is observed with other DEAD-box helicases. The remaining part of the NTR (residues 52 to 78) comprises of a loop and an α-helix located before domain 1. To our knowledge, this is only the second report of structural elements in the NTR of DEAD-box RNA helicases as most of the structures of DEAD-box RNA helicases were obtained using proteins expressed without the NTR. Indeed, the recently solved structure of ADP-bound DDX5 only consists of domain 1 ([33], PDB code; 3fe2). The first report documented an α-helix in the NTR of DDX19 which inserts between domains 1 and 2 to inhibit ATP hydrolysis unless it is displaced by RNA binding [37].

Interestingly, the NTR of DDX5-N inhibits its interaction with NS5B (Figure 7). The α-helix in NTR is essential for this auto-inhibition and seems to mediate the interaction between the highly flexible 1-51 residues in NTR and NS5B binding site in DDX5-N (Figures 7 and 8), presumably located within residues 79-305. Furthermore, DDX5(1-80aa) can bind directly to DDX5(61-614aa) (Figure 8), thus providing further evidence that the flexible NTR of DDX5 folds back to interact with the NS5B binding site. Consistently, NMR investigations reveal that there is indeed a direct interaction between DDX5-NΔ60 and NS5B *in vitro* (Figure 9).

Our results suggest that the DDX5-N and DDX5-C interact with NS5B independently. The high-resolution three-dimensional structure of the apo form of DDX5-N was solved and provides a basis for future studies to define the precise role of

DDX5 during HCV infection. Crystallization of full-length DDX5 and the DDX5-NS5B complex is also actively being pursued. Our data also reveal that the interaction between DDX5-N and NS5B is auto-inhibited by the highly flexible NTR of DDX5-N and the α-helix formed by amino acids 70-78 is necessary for the inhibition to occur. It is expected that solving the structure of full-length DDX5 can help us ascertain whether this α-helix can insert between domains 1 and 2 as has been observed for DDX19 [37].

Recent studies revealed that several DEAD-box RNA helicases, like DDX3, rck/p54 and RNA helicase A, are required for HCV RNA replication [38-40]. It is integrating that multiple DEAD-box RNA helicases are important for HCV replication and further studies are warranted to determine if they are involved in the same step(s) of the viral life-cycle. It is also possible that these host proteins are involved in more than one viral-host interaction. For example, DDX3 not only binds the HCV core protein, but is probably associated with an HCV non-structural protein or HCV RNA itself [38, 41].

References

1 Rosenberg, S. (2001) Recent advances in the molecular biology of hepatitis C virus. J Mol Biol. 313, 451-464

2 Kyono, K., Miyashiro, M. and Taguchi, I. (2002) Human eukaryotic initiation factor 4AII associates with hepatitis C virus NS5B protein in vitro. Biochem Biophys Res Commun. 292, 659-666

3 Tu, H., Gao, L., Shi, S. T., Taylor, D. R., Yang, T., Mircheff, A. K., Wen, Y., Gorbalenya, A. E., Hwang, S. B. and Lai, M. M. (1999) Hepatitis C virus RNA polymerase and NS5A complex with a SNARE-like protein. Virology. 263, 30-41

4 Ford, M. J., Anton, I. A. and Lane, D. P. (1988) Nuclear protein with sequence homology to translation initiation factor eIF-4A. Nature. 332, 736-738

5 Goh, P. Y., Tan, Y. J., Lim, S. P., Tan, Y. H., Lim, S. G., Fuller-Pace, F. and Hong, W. (2004) Cellular RNA helicase p68 relocalization and interaction with the hepatitis C virus (HCV) NS5B protein and the potential role of p68 in HCV RNA replication. J Virol. 78, 5288-5298

6 Fuller-Pace, F. V. (2006) DExD/H box RNA helicases: multifunctional proteins with important roles in transcriptional regulation. Nucleic Acids Res. 34, 4206-4215

7 Cordin, O., Banroques, J., Tanner, N. K. and Linder, P. (2006) The DEAD-box protein family of RNA helicases. Gene. 367, 17-37

8 Linder, P. (2006) Dead-box proteins: a family affair--active and passive players in RNP-remodeling. Nucleic Acids Res. 34, 4168-4180

9 Lane, D. P. and Hoeffler, W. K. (1980) SV40 large T shares an antigenic determinant with a cellular protein of molecular weight 68,000. Nature. 288, 167-170

10 Liu, Z. R. (2002) p68 RNA helicase is an essential human splicing factor that acts at the U1 snRNA-5' splice site duplex. Mol Cell Biol. 22, 5443-5450

11 Abdelhaleem, M. (2005) RNA helicases: regulators of differentiation. Clin Biochem. 38, 499-503

12 Rossler, O. G., Straka, A. and Stahl, H. (2001) Rearrangement of structured RNA via branch migration structures catalysed by the highly related DEAD-box proteins p68 and p72. Nucleic Acids Res. 29, 2088-2096

13 Fuller-Pace, F. V. and Ali, S. (2008) The DEAD box RNA helicases p68 (Ddx5) and p72 (Ddx17): novel transcriptional co-regulators. Biochem Soc Trans. 36, 609-612

14 McGivern, D. R. and Lemon, S. M. (2011) Virus-specific mechanisms of carcinogenesis in hepatitis C virus associated liver cancer. Oncogene. 30, 1969-1983

15 Huang, H., Shiffman, M. L., Cheung, R. C., Layden, T. J., Friedman, S., Abar, O. T., Yee, L., Chokkalingam, A. P., Schrodi, S. J., Chan, J., Catanese, J. J., Leong, D. U., Ross, D., Hu, X., Monto, A., McAllister, L. B., Broder, S., White, T., Sninsky, J. J. and Wright, T. L. (2006) Identification of two gene variants associated with risk of advanced fibrosis in patients with chronic hepatitis C. Gastroenterology. 130, 1679-1687

16   Xiao, J. H., Davidson, I., Matthes, H., Garnier, J. M. and Chambon, P. (1991) Cloning, expression, and transcriptional properties of the human enhancer factor TEF-1. Cell. 65, 551-568

17   Lim, S. P., Khu, Y. L., Hong, W. J., Tay, A., Ting, A. E., Lim, S. G. and Tan, Y. H. (2001) Identification and molecular characterisation of the complete genome of a Singapore isolate of hepatitis C virus: sequence comparison with other strains and phylogenetic analysis. Virus Genes. 23, 89-95

18   Otwinowski, Z. and Minor, W. (1997) Processing of X-ray diffraction data collected in oscillation mode. Methods Enzymol. . 276, 307-326

19   Hogbom, M., Collins, R., van den Berg, S., Jenvert, R. M., Karlberg, T., Kotenyova, T., Flores, A., Karlsson Hedestam, G. B. and Schiavone, L. H. (2007) Crystal structure of conserved domains 1 and 2 of the human DEAD-box helicase DDX3X in complex with the mononucleotide AMP. J Mol Biol. 372, 150-159

20   (1994) The CCP4 suite: programs for protein crystallography. Acta Crystallogr D Biol Crystallogr. 50, 760-763

21   Brunger, A. T., Adams, P. D., Clore, G. M., DeLano, W. L., Gros, P., Grosse-Kunstleve, R. W., Jiang, J. S., Kuszewski, J., Nilges, M., Pannu, N. S., Read, R. J., Rice, L. M., Simonson, T. and Warren, G. L. (1998) Crystallography & NMR system: A new software suite for macromolecular structure determination. Acta Crystallogr D Biol Crystallogr. 54, 905-921

22   Jones, T. A., Zou, J. Y., Cowan, S. W. and Kjeldgaard, M. (1991) Improved methods for building protein models in electron density maps and the location of errors in these models. Acta Crystallogr A. 47 (Pt 2), 110-119

23   Laskowski, R., MacArthur, M., Moss, D. and Thornton, J. (1993) PROCHECK: A program to check the stereochemical quality of protein structures. J. Appl. Crystallogr. . 26, 283-291

24   Qin, H., Noberini, R., Huan, X., Shi, J., Pasquale, E. B. and Song, J. (2010) Structural characterization of the EphA4-Ephrin-B2 complex reveals new features enabling Eph-ephrin binding promiscuity. J Biol Chem. 285, 644-654

25   Qin, H., Shi, J., Noberini, R., Pasquale, E. B. and Song, J. (2008) Crystal structure and NMR binding reveal that two small molecule antagonists target the high affinity ephrin-binding channel of the EphA4 receptor. J Biol Chem. 283, 29473-29484

26   Pace, C. N., Vajdos, F., Fee, L., Grimsley, G. and Gray, T. (1995) How to measure and predict the molar absorption coefficient of a protein. Protein Sci. 4, 2411-2423

27   Delaglio, F., Grzesiek, S., Vuister, G. W., Zhu, G., Pfeifer, J. and Bax, A. (1995) NMRPipe: a multidimensional spectral processing system based on UNIX pipes. J Biomol NMR. 6, 277-293

28   Johnson, B. A. and Blevins, R. A. (1994) NMRView: a computer program for the visualization and analysis of NMR data. J. Biomol. NMR 4, 603–614

29   Carmel, A. B. and Matthews, B. W. (2004) Crystal structure of the BstDEAD N-terminal domain: a novel DEAD protein from Bacillus stearothermophilus. RNA. 10, 66-74

30   Caruthers, J. M., Johnson, E. R. and McKay, D. B. (2000) Crystal structure of yeast initiation factor 4A, a DEAD-box RNA helicase. Proc Natl Acad Sci U S A. 97, 13080-13085

31   Shi, H., Cordin, O., Minder, C. M., Linder, P. and Xu, R. M. (2004) Crystal structure of the human ATP-dependent splicing and export factor UAP56. Proc Natl Acad Sci U S A. 101, 17628-17633

32   Sengoku, T., Nureki, O., Nakamura, A., Kobayashi, S. and Yokoyama, S. (2006) Structural basis for RNA unwinding by the DEAD-box protein Drosophila Vasa. Cell. 125, 287-300

33   Schutz, P., Karlberg, T., van den Berg, S., Collins, R., Lehtio, L., Hogbom, M., Holmberg-Schiavone, L., Tempel, W., Park, H. W., Hammarstrom, M., Moche, M., Thorsell, A. G. and Schuler, H. (2010) Comparative structural analysis of human DEAD-box RNA helicases. PLoS One. 5

34   Jalal, C., Uhlmann-Schiffler, H. and Stahl, H. (2007) Redundant role of DEAD box proteins p68 (Ddx5) and p72/p82 (Ddx17) in ribosome biogenesis and cell proliferation. Nucleic Acids Res. 35, 3590-3601

35   Story, R. M. and Steitz, T. A. (1992) Structure of the recA protein-ADP complex. Nature. 355, 374-376

36   Yang, Z. R., Thomson, R., McNeil, P. and Esnouf, R. M. (2005) RONN: the bio-basis function neural network technique applied to the detection of natively disordered regions in proteins. Bioinformatics. 21, 3369-3376

37   Collins, R., Karlberg, T., Lehtio, L., Schutz, P., van den Berg, S., Dahlgren, L. G., Hammarstrom, M., Weigelt, J. and Schuler, H. (2009) The DEXD/H-box RNA helicase DDX19 is regulated by an {alpha}-helical switch. J Biol Chem. 284, 10296-10300

38   Ariumi, Y., Kuroki, M., Abe, K., Dansako, H., Ikeda, M., Wakita, T. and Kato, N. (2007) DDX3 DEAD-box RNA helicase is required for hepatitis C virus RNA replication. J Virol. 81, 13922-13926

39   He, Q. S., Tang, H., Zhang, J., Truong, K., Wong-Staal, F. and Zhou, D. (2008) Comparisons of RNAi approaches for validation of human RNA helicase A as an essential factor in hepatitis C virus replication. J Virol Methods. 154, 216-219

40   Scheller, N., Mina, L. B., Galao, R. P., Chari, A., Gimenez-Barcons, M., Noueiry, A., Fischer, U., Meyerhans, A. and Diez, J. (2009) Translation and replication of hepatitis C virus genomic RNA depends on ancient cellular proteins that control mRNA fates. Proc Natl Acad Sci U S A. 106, 13517-13522

41   Owsianka, A. M. and Patel, A. H. (1999) Hepatitis C virus core protein interacts with a human DEAD box protein DDX3. Virology. 257, 330-340

Table 1. Data Collection and Refinement Statistics

Data Collection

Wavelength (Å)	0.99
Resolution (Å)[a]	25-2.7 (2.8-2.7)
Space group	*I222*
Unit-cell parameters (Å, °)	a = 66.18, b = 73.80, c = 104.00 $\alpha=\beta=\gamma=90$
Observed reflections[a]	42651 (4083)
Unique reflections[a]	7229 (704)
Completeness (%)[a]	99.8 (99.9)
$I/\sigma(I)$[a]	21.5 (2.7)
R_{merge} (%)[a]	8.5 (48.3)
Multiplicity[a]	5.9 (5.8)

Refinement Statistics

R (%)	27
R_{free} (%)	29

Rms deviation

Bond lengths (Å)	0.008
Bond angles (°)	1.6

Model Quality (Ramachandran Plot)[b]

Residues in most favoured regions (%)	82.3
Residues in additional allowed regions (%)	16.4
Residues in generously allowed and disallowed regions (%)	0.5

[a] Values in brackets indicate values in the highest resolution shell
[b] Values from PROCHECK [23].

Figure legends

Figure 1. Interaction of HCV NS5B with full-length and deletion mutants of DDX5 as determined by coimmunoprecipitation experiments. Huh-7 cells were transfected with cDNA constructs for expressing myc-tagged GST (negative control), myc-tagged full-length or deletion mutants of DDX5 and flag-tagged HCV NS5B. The cells were harvested at 16 h posttransfection, lysed, and subjected to immunoprecipitation with anti-myc polyclonal antibody and protein A agarose beads. The amount of flag-tagged NS5B that coimmunoprecipitated (co-IP) with the myc-tagged proteins was determined by Western blot analysis with an anti-flag monoclonal antibody (top panel). The protein marked with an asterisk represents the heavy chain of the antibody used for immunoprecipitation (top panel). The amounts of myc-tagged and flag-tagged proteins in the lysates before co-IP were determined by subjecting aliquots of the lysates to Western blot analysis (WB, middle and bottom panels).

Figure 2. Structural features of DDX5-N. A ribbon representation of the structure of DDX5-N (residues 52-304). Residues 52-78 (Orange) correspond to a segment from the N-terminal variable region (NTR) whereas the remaining residues 79-304 correspond to the conserved domain 1. Conserved motifs are illustrated accordingly. All structural figures were generated with PyMOL (http://pymol.sourceforge.net/).

Figure 3. Structure based sequence alignment of DEAD-box helicases DDX5, DDX3X, VASA and eIF4a. DEAD-box helicases contain 2 conserved covalently linked globular domains, termed domain1 and 2, flanked by highly variable N and C terminal sequences. Only part of the highly variable N and C terminal sequences is shown. Identical residues are shown in white letters with filled boxes while similar residues are boxed. The conserved domains harbor highly conserved motifs. Domain 1 contains conserved motifs Q, I, II, Ia, Ib and III, whereas domain 2 possess motif IV, V and VI. The conserved motifs are highlighted. Secondary structure elements of DDX5 are shown.

Figure 4. Structural comparison of domain 1 of DDX5 and DDX3X. The apo form of DDX5 is highlighted in green and red whereas the AMP bound form of DDX3X is in blue. The regions highlighted in red (a and b) show the major difference between DDX5 and DDX3X. The P-loop in DDX5 is in a closed conformation (a). Furthermore, DDX5 lacks a 10 amino acid insertion, which forms a helix between the P-loop and motif Ia in DDX3X (b). Despite these differences the main chain atoms of domain 1 of both helicases superimposed with an rmsd of 1.4 Å.

Figure 5. Structural comparison of the apo and ADP bound forms of domain 1 of DDX5. Stereo view of apo (green) and ADP bound forms of DDX5 (pale blue). The P-loop (found in motif I) for the ADP-bound form is highlighted in purple. The P-loop undergoes significant conformation changes upon nucleotide binding. The bound ADP is shown in sticks.

Figure 6. Co-immunoprecipitation of NS5B with DDX5-N containing mutation in the ATP binding or ATP hydrolysis site. Huh-7 cells were transfected with cDNA constructs

for expressing myc-tagged GST (negative control), myc-tagged DDX5-N or myc-tagged DDX5-N containing substitution mutation and flag-tagged HCV NS5B. The cells were harvested at 16 h posttransfection, lysed, and subjected to immunoprecipitation with anti-myc polyclonal antibody and protein A agarose beads. The amount of flag-tagged NS5B that coimmunoprecipitated (co-IP) with the myc-tagged proteins was determined by Western blot analysis with an anti-flag monoclonal antibody (top panel). The protein marked with an asterisk represents the heavy chain of the antibody used for immunoprecipitation (top panel). The amounts of myc-tagged and flag-tagged proteins in the lysates before co-IP were determined by subjecting aliquots of the lysates to Western blot analysis (WB, middle and bottom panels).

Figure 7. Co-immunoprecipitation of NS5B with DDX5-N containing deletion mutation in N-terminal flanking region (NTR). (A) A schematic diagram showing deletion mutants of DDX5-N with modifications in the NTR. The first 51 residues of the NTR are highly disordered, followed by an extended loop structure from 52-69 and an α-helix from amino acids 70-78. (B) Huh-7 cells were transfected with cDNA constructs for expressing myc-tagged GST (negative control), myc-tagged DDX5-N or myc-tagged DDX5-N containing deletion mutation in NTR and flag-tagged HCV NS5B. The cells were harvested at 16 h posttransfection, lysed, and subjected to immunoprecipitation with anti-myc polyclonal antibody and protein A agarose beads. The amount of flag-tagged NS5B that coimmunoprecipitated (co-IP) with the myc-tagged proteins was determined by Western blot analysis with an anti-flag monoclonal antibody (top panel). The protein marked with an asterisk represents the heavy chain of the antibody used for immunoprecipitation (top panel). The amounts of myc-tagged and flag-tagged proteins in the lysates before co-IP were determined by subjecting aliquots of the lysates to Western blot analysis (middle and bottom panels).

Figure 8. GST pull-down of ^{35}S-labelled DDX5(61-614aa) by GST-DDX5(1-80aa). 30 µg of GST or GST-DDX5(1-80aa) were mixed with *in vitro* translated ^{35}S-labelled DDX5(61-614aa). 30 µg of glutathione-sepharose bound fusion proteins used in the pull-down assay were analyzed by SDS-polyacrylamide gel electrophoresis followed by Comassie blue staining to ascertain the purity of the proteins (top panel). An autoradiograph shows the amount of ^{35}S-labeled DDX5(61-614aa) protein bound to GST-DDX5(1-80aa) (lane 3) or GST alone (lane 2) (lower panel). One tenth of the binding input was loaded in lane 1 (bottom panel).

Figure 9. Solution conformation of DDX5(61-305aa) and its binding with NS5B. (A) Far-UV CD spectra of DDX5(61-305aa) (blue) and NS5B (red). (B) One-dimensional ^{1}H NMR spectrum of NS5B. (C) Two-dimensional ^{1}H-^{15}N HSQC spectrum of the ^{15}N-labeled DDX5(61-305aa). (D) One-dimensional ^{1}H NMR spectrum of the DDX5(61-305aa) protein. Red arrows are used to indicate several very up-field resonance peaks resulting from the tight tertiary packing. (E) Superimposition of one-dimensional ^{1}H NMR spectra of the DDX5(61-305aa) in the absence of (blue) and in the presence of NS5B at molar ratios of 1:1 (black); 1:2 (green) and 1:3 (red) (DDX5:NS5B). (F) Superimposition of the simulated (black) and real (red) one-dimensional ^{1}H NMR spectra of the mixture of DDX5(61-305aa) and NS5B at a molar ratio of 1:3 (DDX5:NS5B). The

19

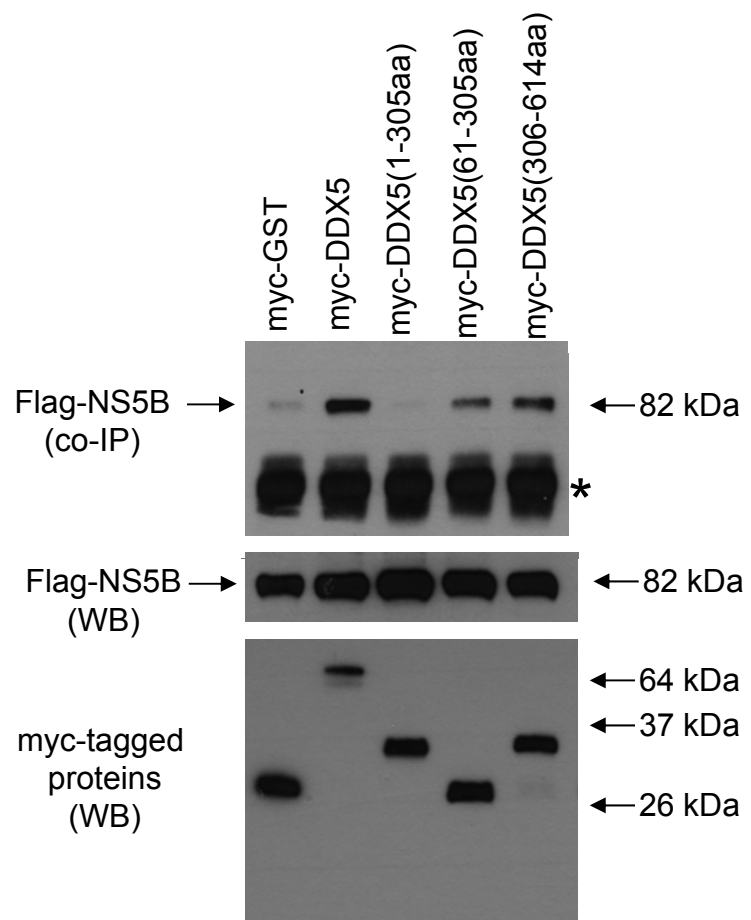simulated spectrum is generated by simply adding up two separate spectra of DDX5(61-305aa) and NS5B at the corresponding concentrations.
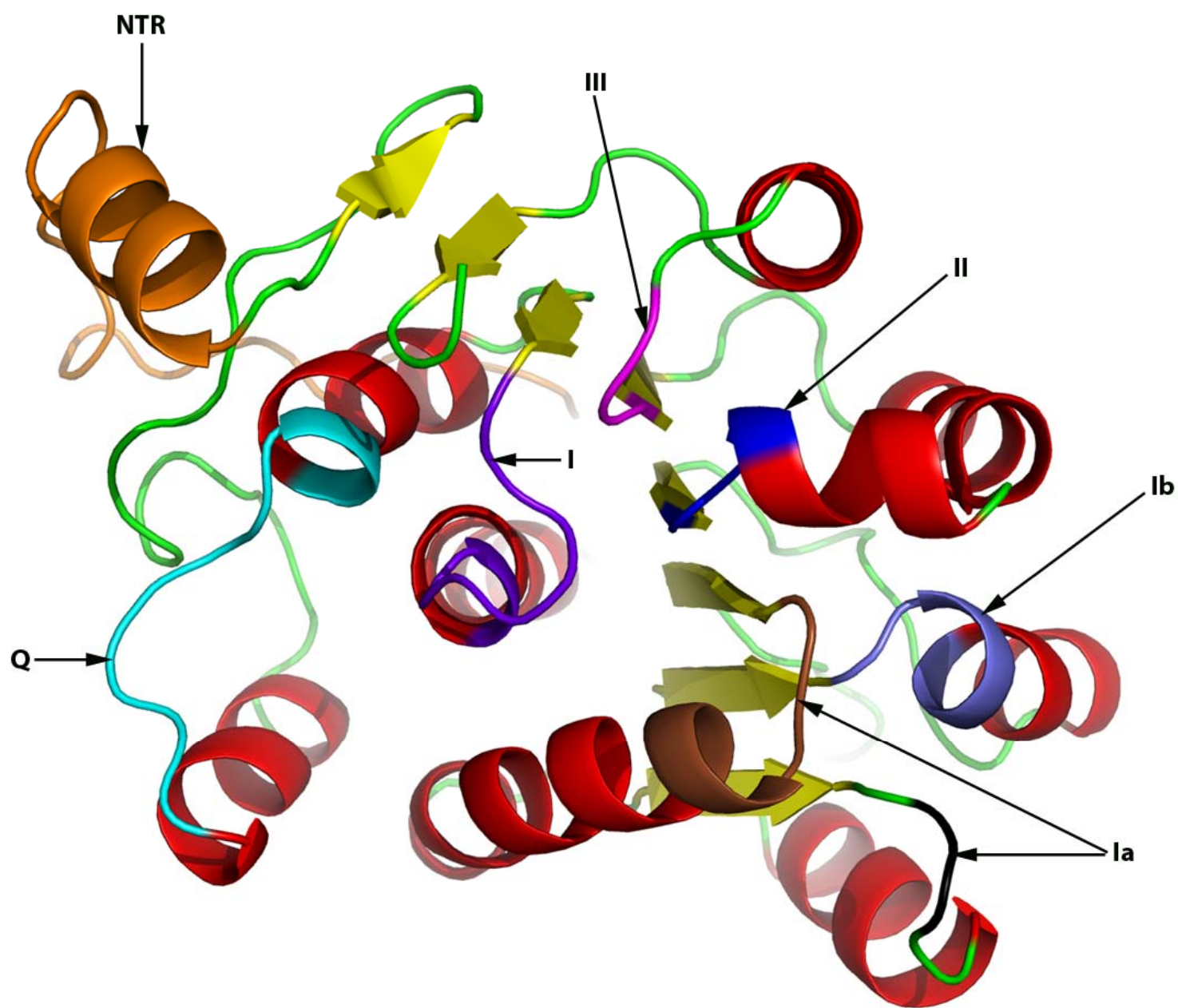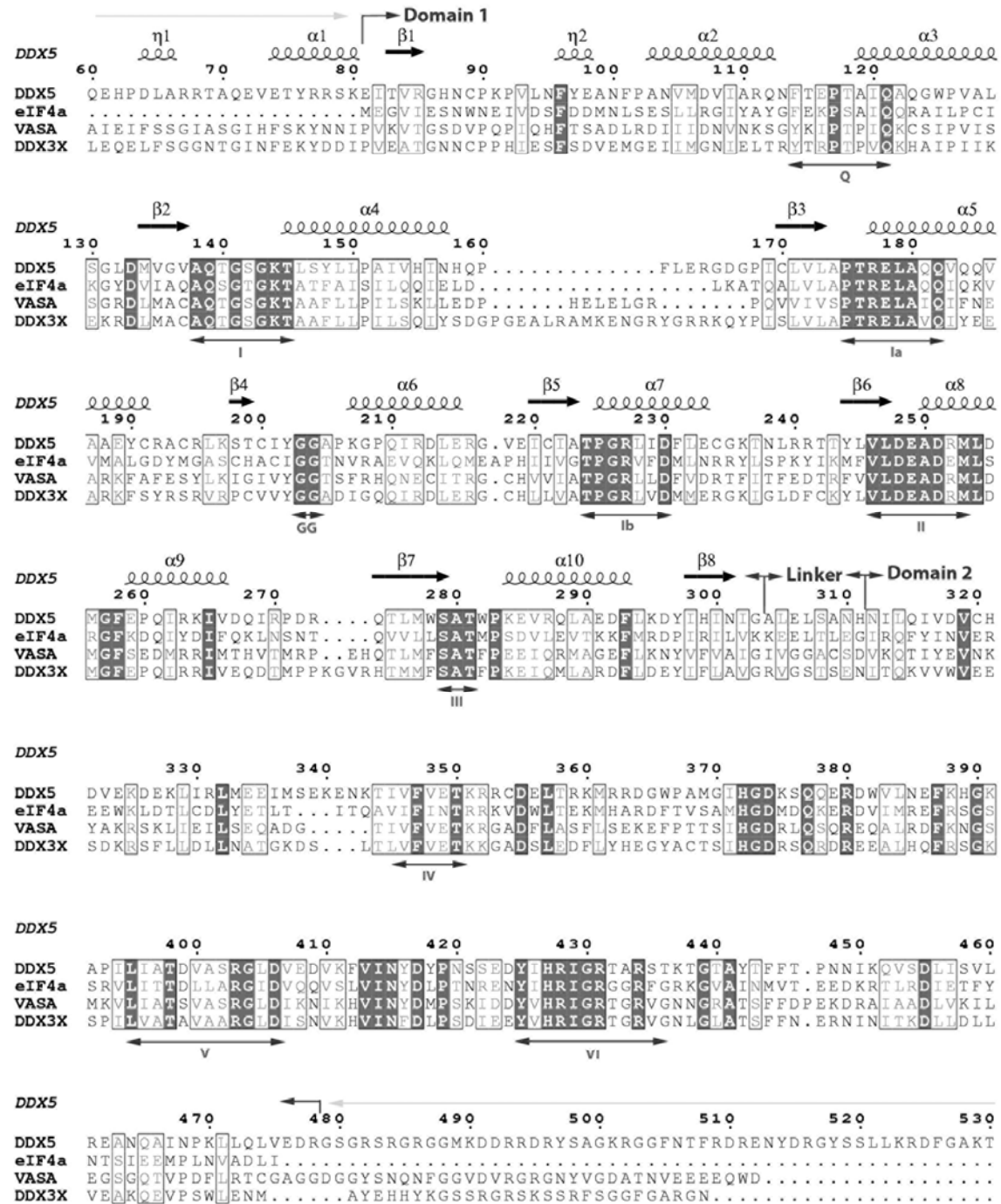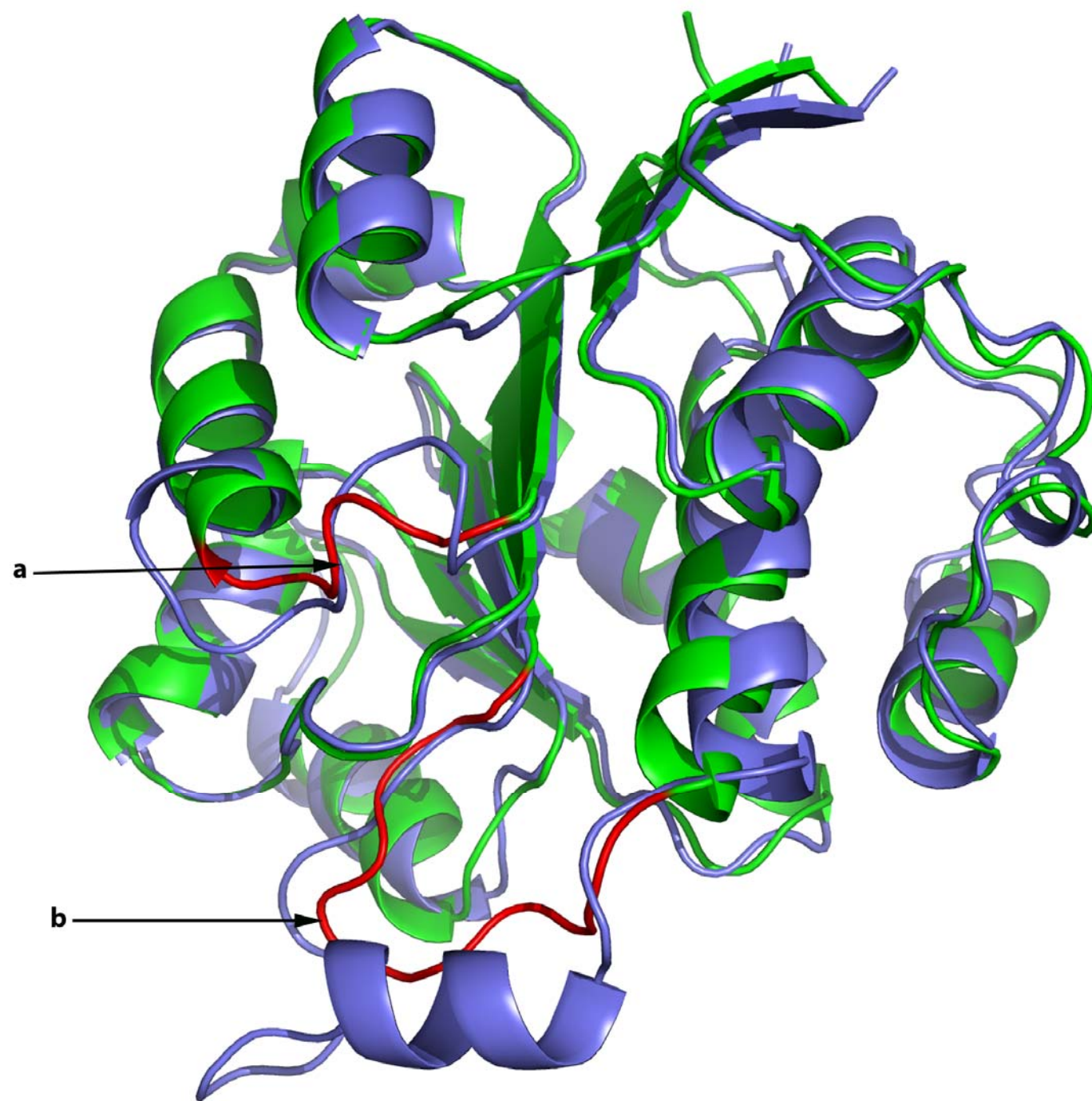
Fig. 1

Fig. 2

Fig. 3

Fig. 4

Fig. 5

Fig. 6

Fig. 7

(A)

DDX5-N   1 ———————————— 305

DDX5-NΔ60aa   61 ————————— 305

DDX5-NΔ78aa   79 ———————— 305

DDX5-N
Δ70-78aa   1 ——————⌃——————— 305

(B)

Flag-NS5B
(co-IP)   ← 82 kDa
                *

Flag-NS5B (WB) ← 82 kDa

myc-tagged
proteins (WB) ← 37 kDa
               ← 26 kDa

myc-GST
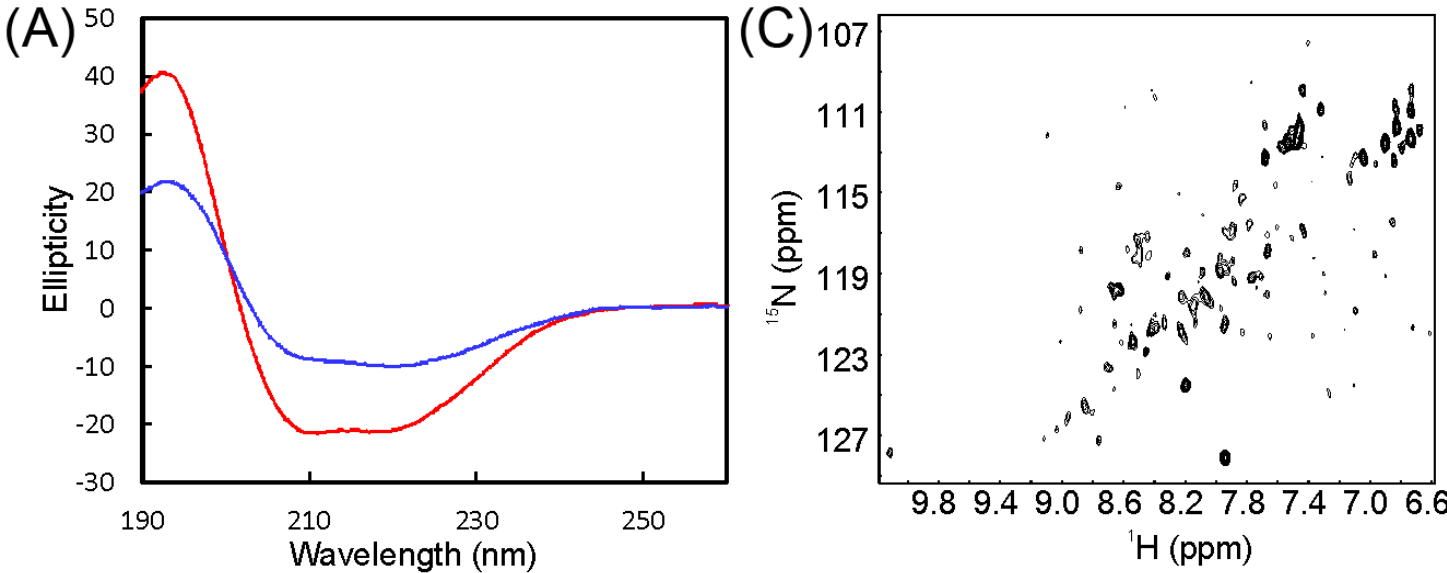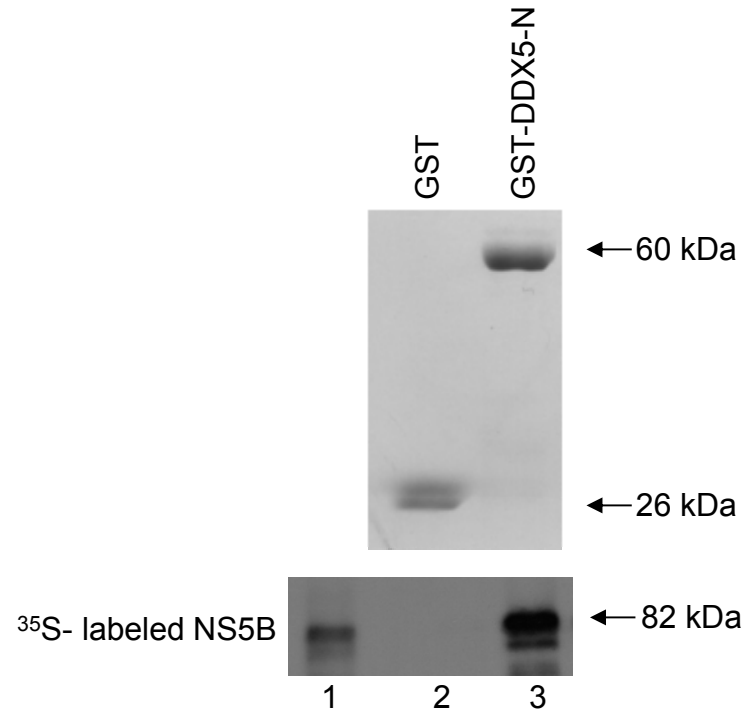myc-DDX5-N
myc-DDX5-ΔN60aa
myc-DDX5-ΔN78aa
myc-DDX5-ΔN70-78aa
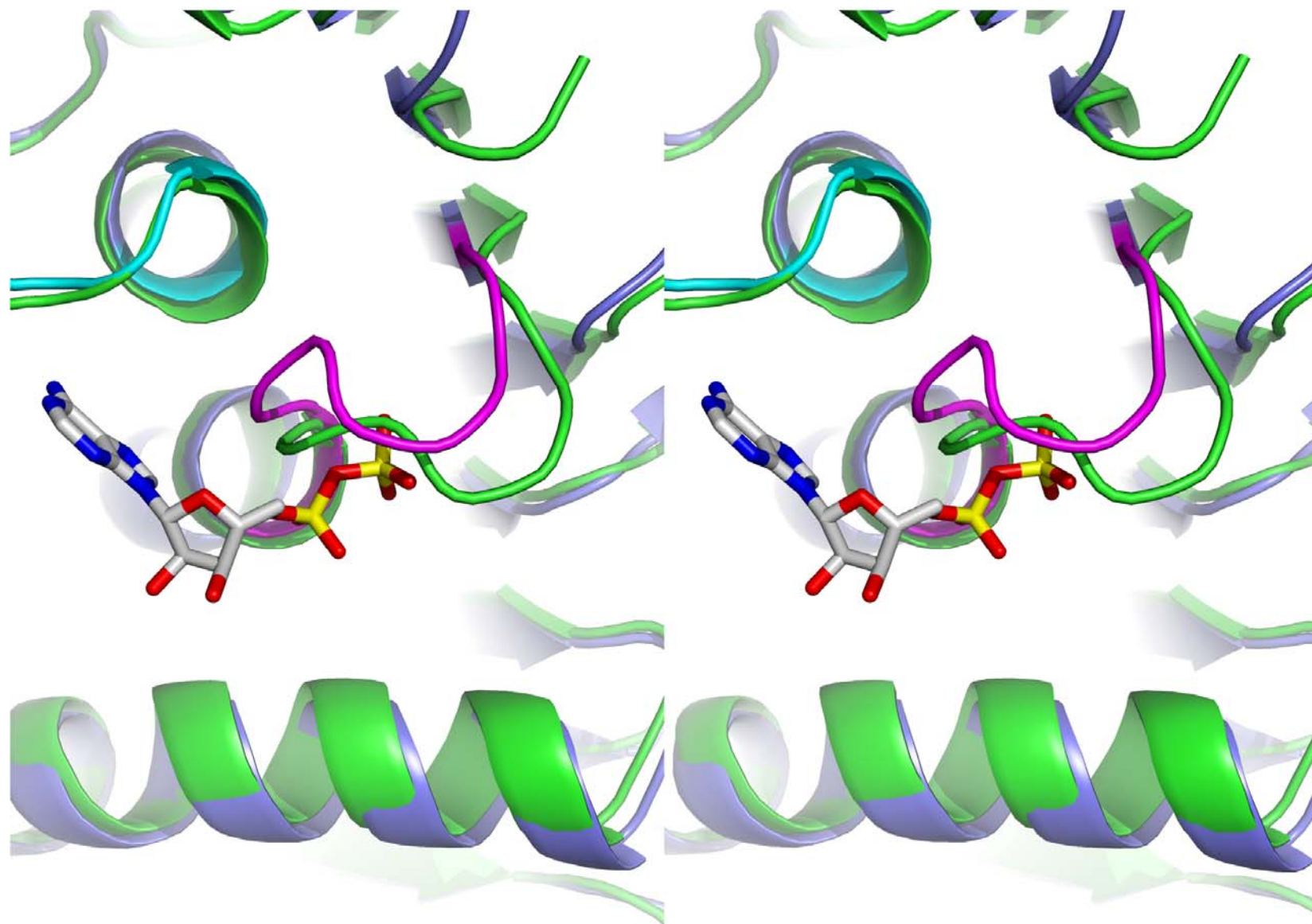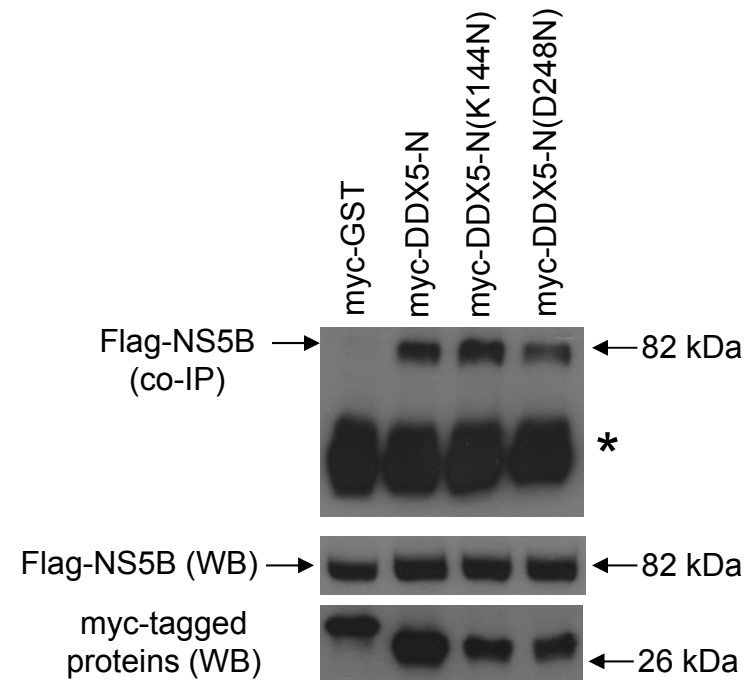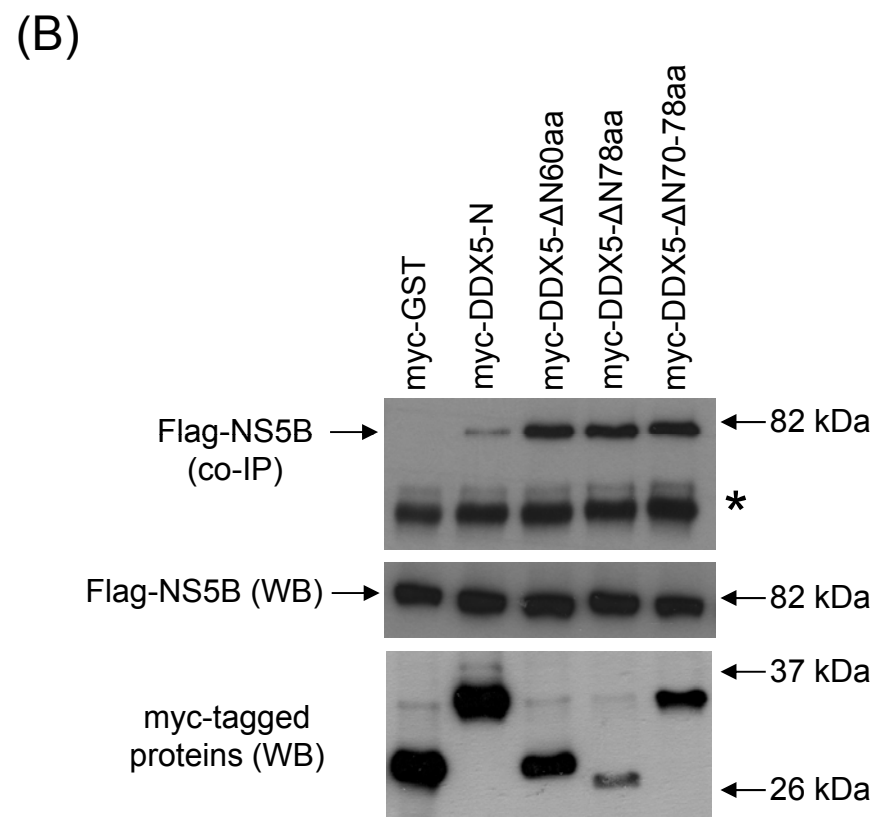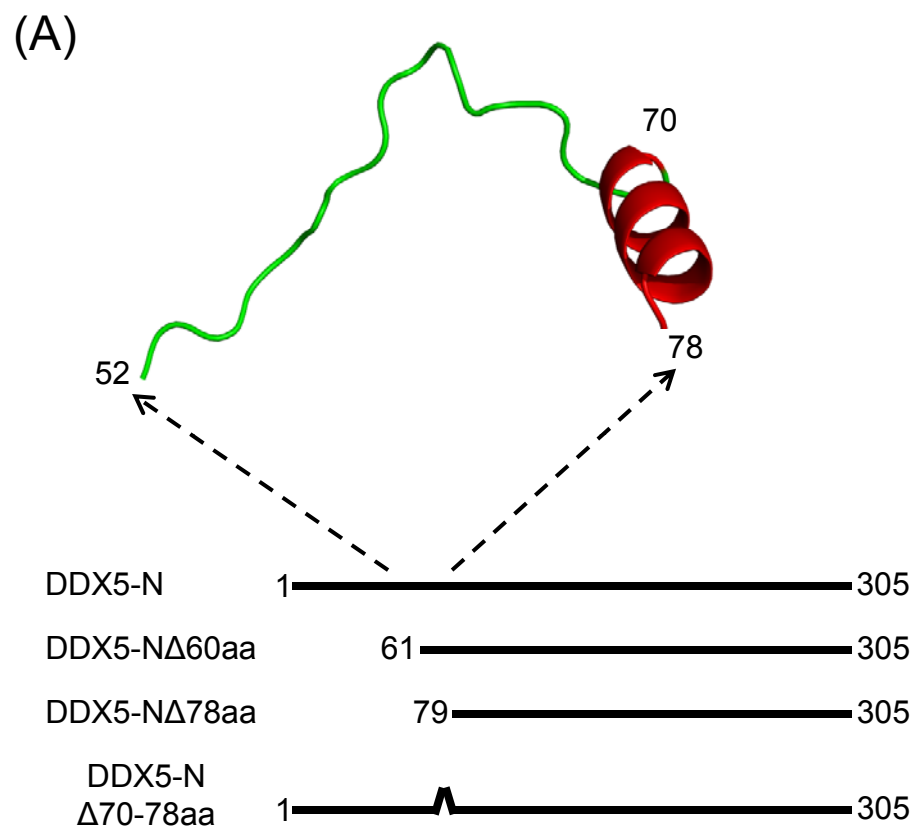
Fig. 8
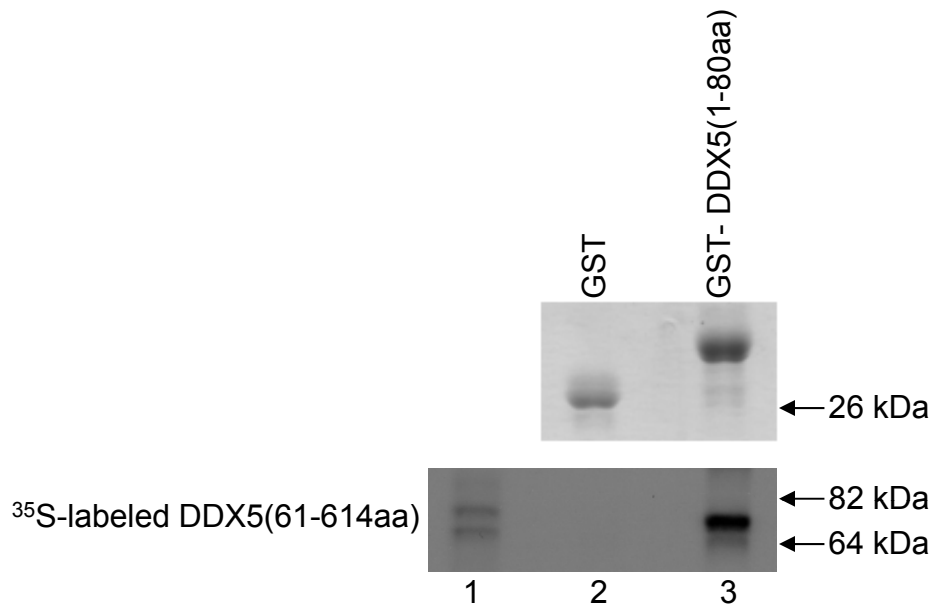
Fig. 9
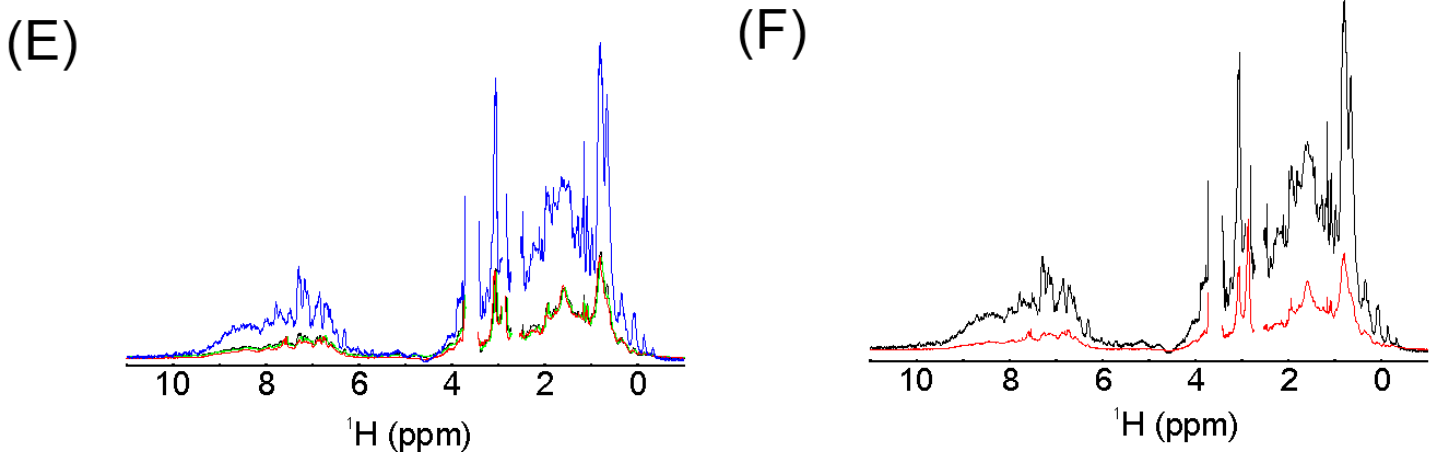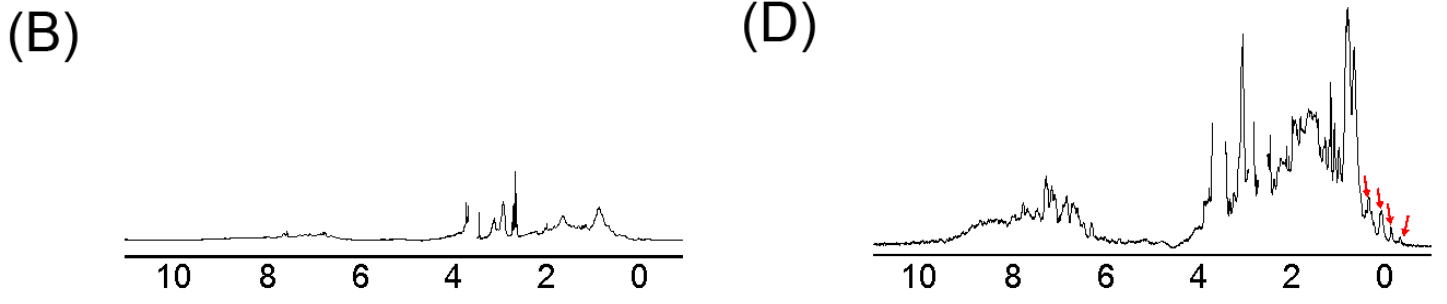
Legend for supplementary Fig.1: GST pull-down of ^{35}S-labelled NS5B by GST-DDX5-N.

30 µg of GST or GST-DDX5-N were mixed with *in vitro* translated ^{35}S-labelled NS5B. 30 µg of glutathione-sepharose bound fusion proteins used in the pull-down assay were analyzed by SDS-PAGE followed by Comassie blue staining to ascertain the purity of the proteins (top panel). An autoradiograph shows the amount of ^{35}S-labeled NS5B protein bound to DDX5-N (lane 3) or GST alone (lane 2) (lower panel). One tenth of the binding input was loaded in lane 1 (lower panel). In contrast to the no or weak binding between DDX5-N and NS5B observed in co-IP experiments (Figure 1 and 7B), the GST-tagged DDX5-N seems to bind NS5B in this GST pull-down experiment. There are two possible reasons for the difference observed in GST pull-down and co-IP experiments. Firstly, the large GST tag of GST-DDX5-N may have caused the NTR to loss its flexibility which is needed for the auto-inhibition effect. Secondly, the sensitivity of the GST pull-down experiment may be higher given that the NS5B protein was isotopically labeled.